

1 **Millennial variability of terrigenous transport to the central-southern** 2 **Peruvian margin during the last deglaciation (18-13 kyr BP)**

3 Marco Yseki¹, Bruno Turcq¹, Sandrine Caquineau¹, Renato Salvattecí², José Solis³, C. Gregory Skilbeck⁴,
4 Federico Velazco⁵ and Dimitri Gutiérrez^{3,5}

5
6 ¹IRD, LOCEAN-IPSL, Laboratoire d'Océanographie et du Climat: Expérimentation et Approches Numériques, Sorbonne
7 Université, CNRS, IRD, MNHN, Paris, France.

8 ²Center for Ocean and Society, Kiel University, Kiel, 24105, Germany.

9 ³Laboratorio de Ciencias del Mar, Facultad de Ciencias y Filosofía, Universidad Peruana Cayetano Heredia, Lima, Peru.

10 ⁴Faculty of Science, University of Technology Sydney. PO Box 123 Broadway, Sydney NSW. 2007.

11 ⁵Dirección General de Investigaciones Oceanográficas y de Cambio Climático, Instituto del Mar del Perú, Callao. Peru.

12 *Correspondence to:* Marco Yseki (marco.yseki@gmail.com)

13 **Abstract.** Reconstructing precipitation and wind from the geological record could help to understand the potential changes in
14 precipitation and wind dynamics in response to climate change in Peru. The last deglaciation offers natural experimental
15 conditions to test precipitation and wind dynamics response to high-latitude forcing. While considerable research has been
16 done to reconstruct precipitation variability during the last deglaciation in the Atlantic sector of South America, the Pacific
17 sector of South America has received little attention. This work aims to fill this gap by reconstructing types of terrigenous
18 transport to the central-southern Peruvian margin (12°S and 14°S) during the last deglaciation (18-13 kyr BP). For this purpose,
19 we used grain-size distribution in sediments of marine core M77/2-005-3 (Callao, 12°S) and G14 (Pisco, 14°S). We analyzed
20 end-members (EMs) to identify grain-size components and reconstruct potential sources and transport processes of terrigenous
21 material across time. We identified four end-members for both Callao and Pisco sediments. In Callao, we propose that the
22 changes in the contributions of EM4 (101 μm) and EM2 (58 μm) mainly reflect the hydrodynamic energy and diffuse sources,
23 respectively, while the variations in EM3 (77 μm) and EM1 (11 μm) reflect changes in the aeolian and fluvial inputs,
24 respectively. In Pisco, where there are strong winds and extensive coastal desert, changes in the contribution of EM1 (10 μm)
25 reflect changes in river inputs while EM2 (52 μm), EM3 (75 μm) and, EM4 (94 μm) reflect an aeolian origin. At millennial-
26 scale, our record shows an increase of the fluvial inputs during the last part of Heinrich Stadial 1 (~ 16-14.7 kyr BP) at both
27 locations. This increase was linked to higher precipitation in Andes related to a reduction of the Atlantic Meridional
28 Overturning Circulation and meltwater discharge in North Atlantic. In contrast, during Bølling-Allerød interstadial (~ 14.7-13
29 kyr BP), there was an aeolian input increase, associated with stronger winds and lower precipitation that indicate an expansion
30 of the South Pacific Subtropical High. These conditions would correspond to a northern displacement of the Intertropical
31 Convergence Zone-South Subtropical High system associated with a stronger Walker circulation. Our results suggest that
32 variations in river discharge and changes in surface wind intensity in the western margin of South America during the last
33 deglaciation were sensitive to Atlantic Meridional Overturning Circulation variations and Walker circulation on millennial

34 timescales. In the context of global warming, large-scale increases in precipitation and fluvial discharge in the Andes as a
35 result of declining of Atlantic Meridional Overturning Circulation and southward displacement of the Intertropical
36 Convergence Zone should be considered.

37 **1. Introduction**

38 The last deglaciation, a period of global warming starting at the end of the Last Glacial Maximum (LGM, ~ 19 kyr BP) to the
39 Early Holocene (11.7 kyr BP), is an outstanding period in the earth's history that provides a better understanding of the
40 mechanisms regulating regional climatic conditions as a consequence of global warming (Clark et al., 2012; Shakun et al.,
41 2012). During the last deglaciation, variations in the meltwater discharge in the North Atlantic and their consequent impact on
42 the intensity of the Atlantic Meridional Overturning Circulation (AMOC) resulted in abrupt climatic changes on a millennial-
43 scale (McManus et al., 2004; Mulitza et al., 2017; Ng et al., 2018), which in turn caused changes in the meridional-oceanic
44 temperature gradient as well as a meridional shift of the mean annual position of the Intertropical Convergence Zone (ITCZ)
45 (Cheng et al., 2012; Deplazes et al., 2013; Mcgee et al., 2014).

46 Numerous studies based on both continental and marine records have evaluated the effects of meltwater discharge and
47 temperature variations in the North Atlantic on precipitation in Tropical South America (TSA) (e.g., Mollier-Vogel et al.,
48 2013; Novello et al., 2017; Mulitza et al., 2017; Strikis et al., 2015, Bahr et al., 2018). Most such studies have suggested wetter
49 conditions in this region during cold events in the North Hemisphere, including the Heinrich Stadial 1 (HS1, ~ 18-14.7 kyr
50 BP) and the Younger Dryas (YD, ~ 12.9-11 kyr BP). This has been linked to a southern displacement of the ITCZ (e.g.,
51 Mollier-Vogel et al., 2013; Mulitza et al., 2017; Bahr et al., 2018) and an intensification of the South American Monsoon in
52 its southern domain (Novello et al., 2017; Strikis et al., 2015) in response to the weakening of the AMOC and increased
53 meltwater discharges into the North Atlantic. Conversely, during the Bølling-Allerød (B-A, 14.7-12.9 kyr BP), a warm period
54 in the North Hemisphere, dry conditions developed in TSA (e.g., Mollier-Vogel et al., 2013; Novello et al., 2017; Mulitza et
55 al., 2017) due to the strong AMOC, the more northerly position of the ITCZ, and the weakening of the South American
56 Monsoon.

57 However, most records covering the last deglaciation concern Eastern South America (e.g., Cruz et al., 2005; Montade et al.,
58 2015; Strikis et al., 2015; Zhang et al., 2015; Novello et al., 2017, Mulitza et al., 2017; Bahr et al., 2018; Strikis et al., 2018),
59 while records from the western slope of the Andes (e.g., Baker et al., 2001a, 2001b) and the Peruvian margin are scarce (e.g.,
60 Rein et al., 2005; Mollier-Vogel et al., 2013). Previous attempts to reconstruct changes in the precipitation in the western flank
61 of the Andes using marine sediment records have given rise to contrasting results. In Northern Peru (4°S), based on titanium
62 (Ti) to calcium (Ca) ratios, Mollier-Vogel et al. (2013) suggest an increase in fluvial inputs during the HS1 and YD and reduced
63 precipitation during the B-A. However, off Callao (12°S), no difference in fluvial inputs, here based on lithic content, between
64 HS1 and BA is reported (Rein et al., 2005). The difference between the two records could be because of the changes in sediment
65 transport at the two sites and/or to the interpretation of the proxies used in these studies. In both studies, Ti/Ca ratio at 4°S

66 (Mollier-Vogel et al., 2013) and lithic content at 12°S (Rein et al., 2005) were considered as indicators of the fluvial inputs.
67 The latter, is generally true in Northern Peru (4°S) where rainfall can reach 466 mm y⁻¹ (Lagos et al., 2008). However, other
68 processes can be invoked in more arid regions, for example, in central-southern Peru where rainfall is scarce (less than 20 mm
69 y⁻¹) (Lagos et al., 2008). Indeed, Briceño-Zuluaga et al. (2016) have shown that, during the last millennium, part of the detrital
70 fraction of marine sediments collected off Pisco was also of aeolian origin. According to Briceño-Zuluaga et al. (2016) aeolian
71 inputs off Pisco can contribute up to almost 50% of the terrigenous fraction during some climatic periods (e.g., the Medieval
72 Climatic Anomaly). These results are based on the grain size distributions of terrigenous components in the sediment.
73 The grain-size distribution of Peruvian margin sediments is typically polymodal, and for this reason, it can information on
74 sediment transport mechanisms and/or sediment sources (Briceño-Zuluaga et al., 2016). Aeolian particles diameters are
75 relatively coarser than fluvial ones and if wind intensification occurs, the aeolian flow and the frequency of coarse particles (~
76 >36 μm) would increase. Thus, the relative abundance of fluvial particles (~ 6-14 μm) would reflect the precipitation and
77 continental runoff (e.g., Stuut et al., 2002; Stuut and Lamy 2004; Pichevin et al., 2005; Briceño-Zuluaga, et al., 2016; Beuscher
78 et al., 2017). Mathematical methods can be to identify the grain-size components of polymodal sediments. For instance, end-
79 member analysis (EMA) has been widely used to infer changes in fluvial and/or aeolian inputs (e.g., Stuut et al., 2002, 2004,
80 2007, 2014; Weltje y Prins, 2003; 2007; Pichevin et al., 2005; Holz et al., 2007; Just et al., 2012; Beuscher et al., 2017;
81 Humphries et al., 2017; Jiang et al., 2017).

82 The aim of the current work is to reconstruct at the millennial-scale the transport (fluvial and aeolian) and sedimentation of
83 the terrigenous inputs off central-southern Peru (Callao and Pisco) during the last deglaciation. To achieve this, grain size
84 distributions on surface sediments and sediments cores (M77/2-005-3, Callao and G14, Pisco) were measured and EMA was
85 used to deconvolved them into subpopulations. Surface sediments were collected during normal conditions and during the
86 2017 Coastal El Niño (April 2017). During the 2017 Coastal El Niño, the flow of the Callao and Pisco Rivers reached extremely
87 high levels during austral summer 2017, especially during March 2017 (Guzman et al., 2020). Likewise, in the month of April
88 2017, wind surface anomalies were positive, especially in Central and Southern Peru (Echevin et al., 2018). Chamorro et al.
89 (2018) found a quasi-linear relationship between surface wind and pressure gradient anomalies during the El Niño period in
90 1998. The alongshore pressure gradient anomalies, in 1998, were caused by a greater increase in near-surface air temperature
91 off the northern coast than off the southern coast of Peru. This inhomogeneous sea surface warming is similar during El Niño
92 2017. Based on the above, the samples collected in April 2017 may reflect changes in fluvial and maybe aeolian transport
93 associated with Coastal or East Pacific El Niño events.

94 In addition, as a proxy for fluvial vs aeolian inputs, we used the titanium/zirconium (Ti/Zr) record from X-Ray fluorescence
95 (XRF) analysis of the 106KL core collected off Callao and described by Rein et al. (2005). In a subsequent step, Ti, Al and Zr
96 were measured in surface sediments at Callao and Pisco by ICP-MS to better interpret the XRF results. We postulate that
97 changes in the AMOC intensity have modulated the variability of winds and precipitation in the Western TSA, as inferred by
98 changes in the grain-size distribution of marine sediment particles, at millennial time-scales. Our work provides new
99 information on sedimentation, types of transport and sources of terrigenous inputs on the Peruvian margin during the last

100 deglaciation, offering a better understanding of the mechanisms modulating these processes during past periods of global
101 warming.

102 **1.2 Regional setting**

103 We focused on the central-southern part (12-14°S) of the Peruvian margin. Callao and Pisco are located onshore in the Lima
104 Basin (Suess et al., 1987). This basin exhibits high productivity and anoxic conditions that are favored by an intense oxygen
105 minimum zone between about 200 and 400 meters depth (Cardich et al., 2019); hence, sediments are composed of fine grains,
106 are rich in organic matter, and contain abundant diatoms. The general absence of bioturbation in some areas and during some
107 time periods allows for the preservation of laminations and, therefore, their use as palaeoceanographic records (e.g., Rein et
108 al., 2005; Gutiérrez et al., 2006, 2009, 2011; Sifeddine et al., 2008; Salvattecí et al., 2014a, 2016, 2019; Briceño-Zuluaga et
109 al., 2016;). In Callao, muddy laminated areas are reported (Reinhardt et al., 2002), but sedimentary records collected in the
110 OMZ core, off Pisco, show more continuous laminations than the records collected off Callao (e.g., Salvattecí et al., 2016,
111 2019).

112 The main transport of the detrital fraction of coarse silt and sand to the hemipelagic sediments in the Peruvian margin occurs
113 by the action of winds (Scheidegger and Krissek, 1982). In contrast to Callao, Pisco is characterized by the presence of large
114 coastal deserts, extreme aridity and dust storms known as Paracas winds. During these sporadic sand storms, wind velocities
115 can exceed 10-15 m/s (Briceño-Zuluaga et al., 2017); these storms are produced by the local intensification of alongshore
116 surface wind and by alongshore pressure gradients (Briceño-Zuluaga et al., 2017). Moreover, in Pisco, an intense coastal
117 upwelling linked to strong alongshore surface wind occurs (Dewitte et al., 2011; Gutiérrez et al., 2011; Rahn and Garreaud,
118 2013). The intensity of alongshore surface winds presents a seasonal variability, with stronger winds during austral winter and
119 weaker winds during austral summer (Fig. 1). This seasonality is linked regionally to the displacements of the ITCZ-South
120 Pacific Subtropical High (SPSH) system and locally to continental-oceanic and alongshore pressure gradients (Strub et al.,
121 1998; Gutiérrez et al., 2011; Chamorro et al., 2018). In contrast to the coarser particles that are transported by winds, quartz-
122 rich silt and clays are transported by rivers to the continental shelf (Scheidegger and Krissek, 1982). The central-southern
123 Peruvian coast is characterized by very low annual precipitations (Callao, 14 mm y⁻¹ and Pisco, 2 mm y⁻¹) and intermittent
124 flows of coastal rivers (Lagos et al., 2008). However, during austral summer, there is an increase in river discharges associated
125 with increased monsoon precipitation in the Andes (Garreaud et al., 2009; Vuille et al., 2012). Occasional floods occur and
126 higher sediment discharges are associated with intense precipitation during extreme El Niño events (Bourrel et al., 2015;
127 Morera et al., 2017; Rau et al., 2016; Guzman et al., 2020).

128 A large fraction of the particles smaller than 10 µm (desert aerosols) are transported beyond the continental shelf (Saukel et
129 al., 2011). Therefore, the fine fraction of aeolian origin in the continental shelf sediments is therefore negligible, and the fine
130 fraction of the continental shelf is largely dominated by fluvial inputs. On the other hand, coarser particles (e.g., > 40 µm)
131 settle on the continental shelf (Scheidegger and Krissek, 1982). Once in the water column, the dispersion patterns of clays (<
132 4 µm) and fine silts (8-11 µm) coincide with the surface and subsurface currents, while the coarser fraction presents limited

133 dispersion near the coast (Scheidegger and Krissek, 1982). Likewise, near-bottom processes and bottom topography exert
134 considerable control over the dispersal of hemipelagic sediments on the Peruvian margin (Scheidegger and Krissek, 1982).

135 **2. Materials and methods**

136 **2.1 Surface sediments, marine core and age model**

137 Surface sediments (0-0.5 cm) were collected in front of Callao (N=12) and Pisco (N=9) at depths of 92-178 m and 120-311 m,
138 respectively, by the Instituto del Mar del Peru during the years 2015 (December), 2016 (August and December) and 2017
139 (February, April and, August), specifically along transects perpendicular to the coast (Fig. S1). Details of the sampling sites
140 are given in Table S1. The samples collected in April 2017 coincided with the occurrence of a Coastal El Niño event, and will
141 be considered as representative of “Coastal El Niño” conditions hereafter. All the other samples will represent “normal”
142 conditions.

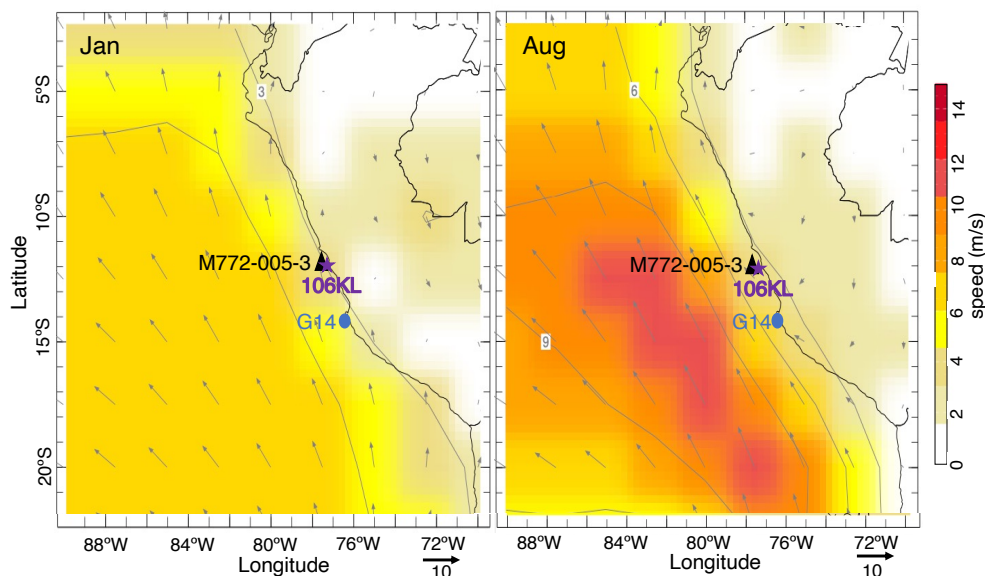
143 The core M77/2-005-3, was retrieved from the Southeast Pacific continental slope (12°05 S, 77°40,07 W, 214 m water depth,
144 1336 cm long) during the M77-2 expedition in 2008 (Fig. 1). Because we focus on the last deglaciation period, we worked
145 with the section from 0 to 700 cm core depth. A first depth-age model based on four ¹⁴C ages was built by Salvattecí et al.
146 (2019). In the present, we added 22 ¹⁴C ages and developed a new age depth-age model (Table S2). Radiocarbon measurements
147 were performed on organic matter at the Laboratoire de Mesures du Carbone-14 (LMC14, Gif-sur Yvette, France). Ortlieb et
148 al. (2011) reported a regional reservoir effect (ΔR) of 511 ± 278 years for the Early Holocene (10.4-6.8 kyr) and in the absence
149 of ΔR data for older periods, we used this value to calibrate the ¹⁴C measurements for the last deglaciation as in Salvattecí et
150 al. (2016, 2019). To construct the age model, we used the maximum probability ages obtained from the CALIB 8.1 software
151 using the Marine 20 dataset. The chronological model based on the lineal model indicates that the examined section (0-700
152 cm) of core M77/2-005-3 (Fig. S2) recorded the LGM and the last deglaciation (22-13 kyr BP; 95-700 cm). Core M77/2-005-
153 3 presents a hiatus at 94 cm, so a great part of the Holocene is missing.

154 Core G14 (14°S, 76°W, 390 m water depth) was retrieved during the Galathea-3 expedition in 2007 (Salvattecí et al., 2016).
155 The radiocarbon dates of G14 were published in Salvattecí et al. (2016). For the current study, a new depth-age model based
156 on a lineal model was developed with an updated calibration using the CALIB 8.1 software and the Marine 20 dataset. The
157 upper part of sediment layers was not recovered in G14, which ranges from 13.4 to 24.6 kyr BP (Fig. S2).

158 The lithological descriptions of M77/2-005-3 and G14 are available in Salvattecí et al. (2016, 2019). The M77/2-005-3 and
159 G14 cores show laminated and banded sediments with no evident signs of major discontinuities during the last deglaciation
160 (Salvattecí et al., 2016, 2019). The G14 core presents more continuous laminated sediments compared with the M722-005-3
161 core. (Salvattecí et al., 2016, 2019).

162 To compare our new data from cores M77/2-005-3 and G14 with previously published records in the area we modified the age
163 model of core 106 KL (Rein et al., 2005). Core 106 KL (12°030S, 77°39.80W, 184 m water depth) was retrieved during cruise
164 SONNE 147 (Rein et al., 2004, 2005). The chronology model and lithology have been fully described in Rein et al. (2004,

165 2005). A new depth-age model based on a lineal model was developed with an updated calibration using the CALIB 8.1
166 software and the Marine 20 dataset (Fig. S2) and we only used the sections covering the last deglaciation.
167



168
169 **Figure 1. (A) Location of the sampling of the sediment cores M77/2-005-3, 106KL and G14 core. Average wind speed (m/s) at 1000**
170 **hPa in January and August (<http://iridl.ldeo.columbia.edu>).**

171

172 2.2 Grain-size distribution and end-member analysis

173 To reduce the effect of sediment disturbances that can produce artificial results, only laminated and banded sequences were
174 subsampled for grain-size distribution analysis. Reworked sediments are widespread in the marine sediment records off Peru
175 and can be distinguished from well-preserved sediments using X-ray images (Salvatteci et al., 2014b). For both surface and
176 core sediment samples, to isolate the terrigenous fraction, we followed the procedure described in Briceño-Zuluaga et al.
177 (2016). Organic matter, calcium carbonates and biogenic silica were successively removed with hydrogen peroxide (H₂O₂ 30%
178 at 60°C for 3 to 4 days), hydrochloric acid (HCl 10% for 12h), and sodium carbonate (Na₂CO₃, 1M at 90°C for 3h), respectively.
179 The grain-size distribution was then measured using an automated image analysis system (model FPIA3000, Malvern
180 Instruments), here with a measurement range of 0.5-200 μm. Further details on the FPIA3000 are described in Flores-
181 Aqueveque et al. (2014) and Briceño-Zuluaga et al. (2016). Given that only particles smaller than 200 μm could be measured
182 under the analytical conditions applied in the present work, all samples were sieved with a 200 μm mesh before being analyzed.
183 Particles larger than 200 μm were not recovered in any sample; thus, our analysis covers the full range of grain size present in
184 the surface and cores sediments.

185 The grain-size distribution was generally plurimodal and for this reason we have used AnalySize modelling algorithm
186 (Paterson and Heslop, 2015), to deconvolute the grain-size distributions; the algorithm establishes a physical mixing model
187 that transforms the measured particle size distribution histograms into the sum of a limited number of end members (Ems)
188 with an unimodal particle size distribution. The sum of determination coefficients (r^2), which represent the proportion of the
189 variance of each EM against the total granulometric distribution, is calculated to estimate the minimum number of EMs
190 necessary to reach a high percentage of the total variance. More specific details are available in Paterson and Heslop (2015).

191 **2.3 ICP-MS analysis**

192 The Al, Ti, and Zr concentrations in the surface sediments were determined by inductively coupled plasma mass spectrometry
193 (ICP-MS) (Agilent 7500 cx) after hot-plate acid digestion in polytetrafluoroethylene (PTFE) vessels. The employed acids (HF,
194 HNO₃, and HClO₄) eliminated organic material and solubilized silicates (Jarvis et al., 1992). The complete protocol is
195 described in details in Salvattecì et al. (2014a). The accuracy of the concentration measurements was determined by
196 comparison with MESS-3 (Marine sediment reference material, National Research Council of Canada). The relative standard
197 deviation (RSD) estimated from duplicate analysis was less than 3.5 % for Al, Ti, and Zr.

198

199 **2.4 XRF analysis**

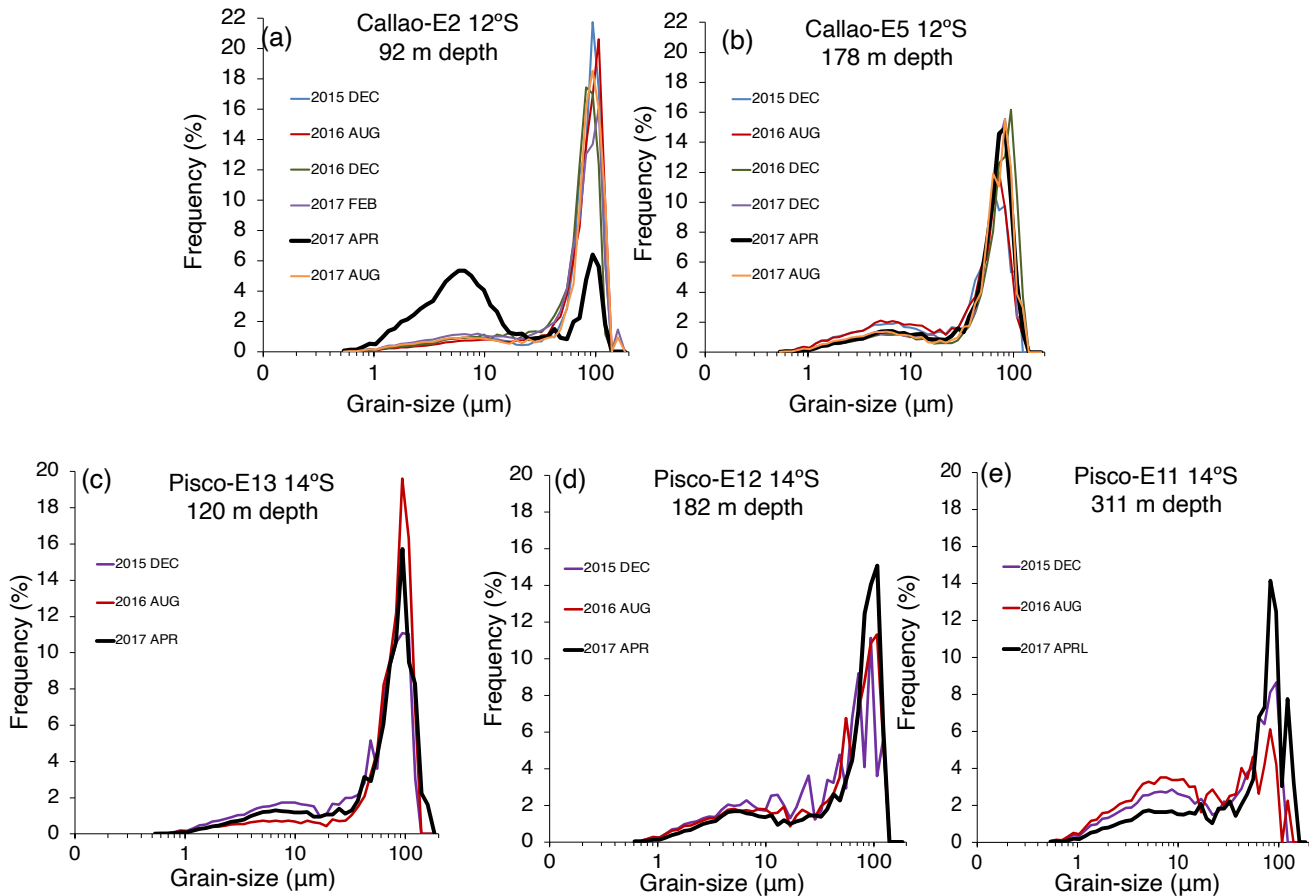
200 The piston core KL 106 was analyzed using an Avaatech XRF Core Scanner at the Marum Center (Bremen). Here, XRF
201 scanning was done for 19 elements at 2-mm intervals. Ti is an aluminum/silicate-related element and is associated mainly with
202 clay minerals transported from the continent to the ocean through river discharges (Jansen et al., 1998; Yarincik et al., 2000).
203 Conversely, Zr is predominantly enriched in heavy mineral species, in particularly zircon. The latter is broadly distributed in
204 natural sediments and typically has a relatively coarse grain size (Pettijohn, 1941). Zr has been widely used as a proxy for
205 mean depositional grain-size variations (e.g., Dypvik and Harris, 2001; Wu et al., 2020). Using the Ti/Zr ratio, we compared
206 Ti, which is present in all sizes of sediment, but especially in clays, to Zr, which would only be present in the silt and sand
207 fractions in the form of zircon minerals. Assuming that fine particles, such as clays, are mainly transported by rivers, while
208 coarse particles (coarse silts and sands) come mainly from an aeolian origin, the Ti/Zr ratio can be used as a potential proxy
209 for fluvial versus aeolian inputs.

210 **3. Results**

211 **3.1 Grain-size distribution of the surface sediments**

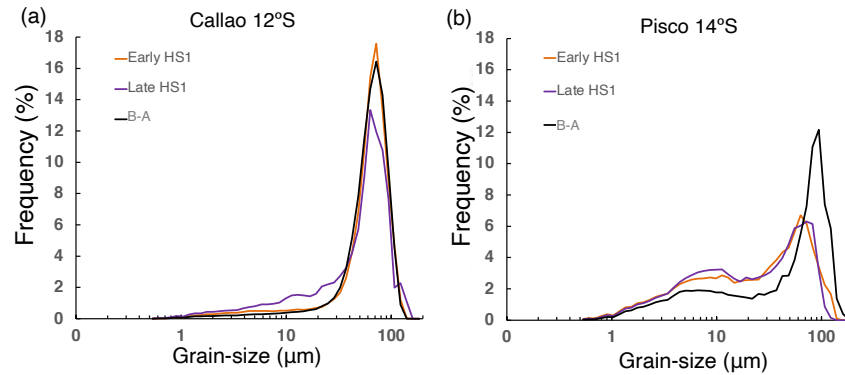
212 The grain-size distribution of all surface samples collected at the stations in Callao and Pisco are shown in Fig. 2. In Callao
213 and Pisco, during normal conditions, the abundance of fine particles (< 10 μm) was higher at the deepest and furthest offshore
214 stations than at coastal stations, while, coarse particles (60-120 μm) were more abundant close to the coast (Fig. 2). Coarser

215 particles were deposited mainly on the inner continental shelf because of their weight. During the 2017 Coastal El Niño, a
216 strong increase in fine particles ($< 10 \mu\text{m}$) abundance was found only at station E2 (Fig. 2a) in Callao. On the other hand, the
217 abundance of the coarse fraction ($50\text{-}100 \mu\text{m}$) in the sediments from the most distant stations (E12 and E11) increased in Pisco
218 (Fig. 2d and 2e).
219



220
221 **Figure 2. Grain-size distribution of surface sediments at the Callao (a, b) and Pisco stations (c, d, e).**

222
223 The mean grain-size distribution per climatic period analyzed is shown in Fig. 3a and 3b. During the Late HS1 (16-14.7 kyr
224 BP), the abundance of fine particles ($< 10 \mu\text{m}$) was higher than during the Early HS1 (18-16 kyr BP) and B-A in Callao and
225 Pisco (Fig. 3a and 3b). This increase was more pronounced in Callao (Fig. 3a). On the other hand, during the B-A (14.7-13
226 kyr BP), the sediments were characterized by a high abundance of coarser particles (Fig 3a and 3b).
227



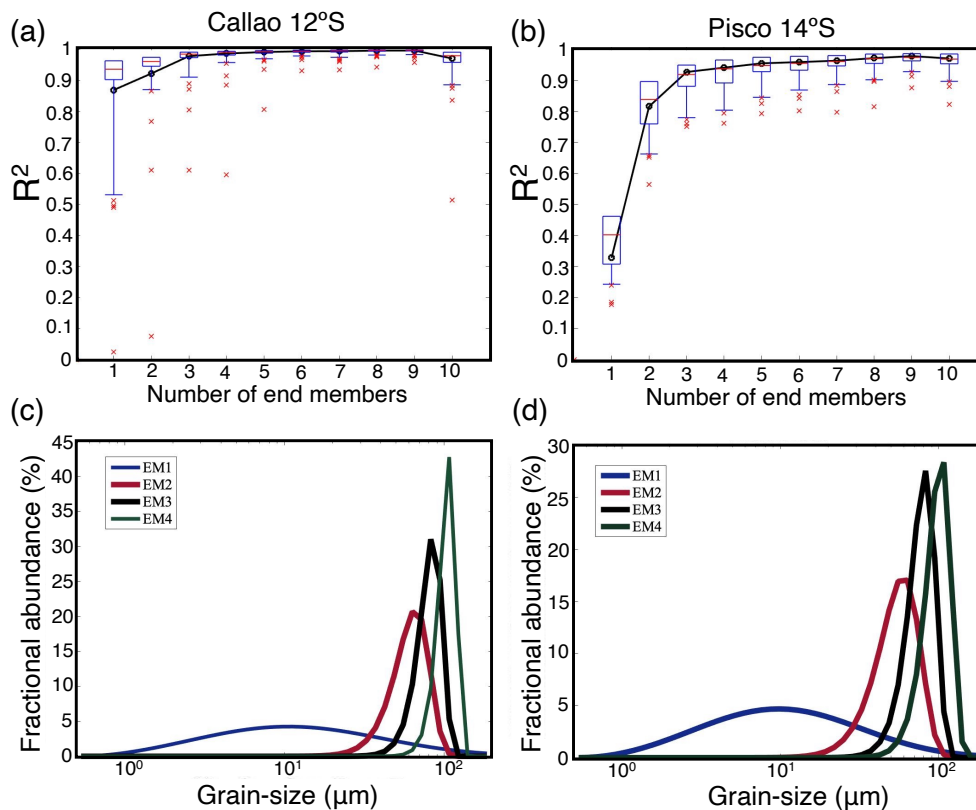
228
 229 **Figure 3. Mean grain-size distribution by climatic period in Callao (a) and Pisco (b).**

230

231 **3.2 End-member analysis**

232 Based on a multiple correlation coefficient, a model with four EMs was chosen in Callao and Pisco, which explained 98% and
 233 95% of the variance of the grain-size distribution data set, respectively (Fig. 4a and 4b). The measured and modeled grain-size
 234 distribution were highly correlated (R^2 : 0.86-0.99) for each analyzed sample, attesting to the fact that the use of four EMs was
 235 appropriate for our interpretation. Although a model with two EMs model explained 95% of the variance of the data in Callao,
 236 the variability of each EM's contribution was different (Fig. 6), suggesting that each EM indicated different processes or
 237 sources. Each of the four EMs presented a unimodal distribution, with its median being respectively at 11 μm (EM1), 58 μm
 238 (EM2), 77 μm (EM3) and 101 μm (EM4) in Callao (Fig. 4c). In Pisco, each EM was represented by a unimodal distribution
 239 centered at 10 μm (EM1), 52 μm (EM2), 75 μm (EM3) and 94 μm (EM4) (Fig. 4d).

240



241

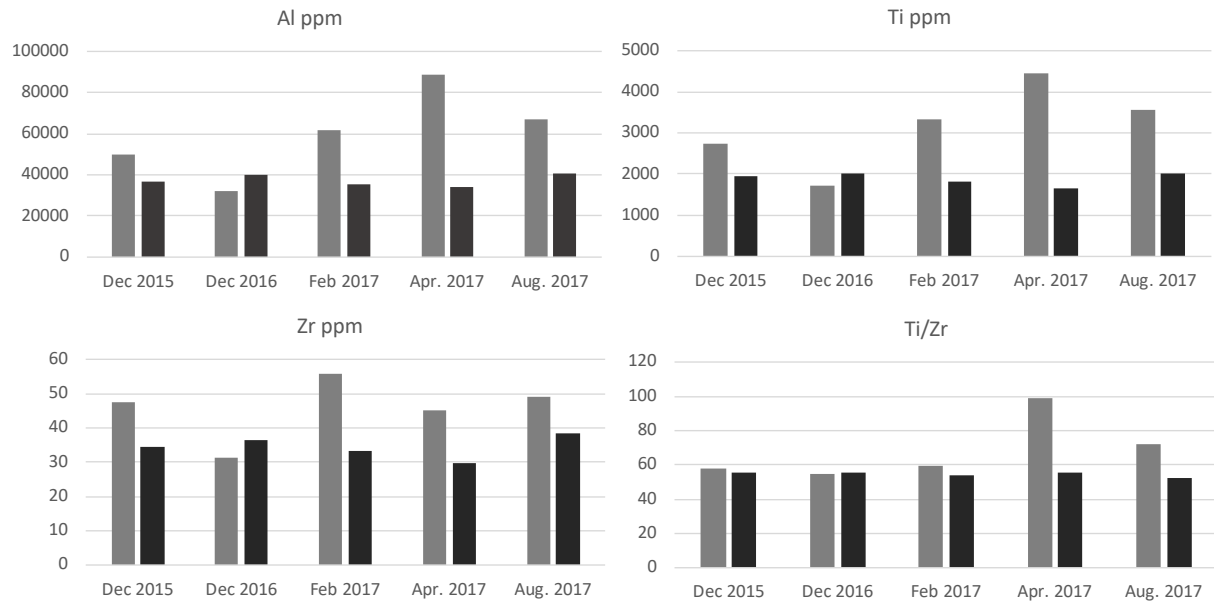
242 **Figure 4. Coefficient of determination (r^2) as a function of the number of end members chosen to model the observed grain-size**
 243 **distribution in Callao (a) and Pisco (b). Grain size distribution of the four end-members in Callao (c) and Pisco (d).**

244

245 3.3 ICP-MS and XRF analysis

246 The concentrations of Al, Ti, Zr, and Ti/Zr ratio of the surface samples collected at Callao are presented in Fig. 5. The E2
 247 station in Callao showed a very large increase in Ti and Al during the Coastal El Niño (April 2017), with values twice the
 248 average of all other samples. This was related to the large amount of fine particles measured that month in Callao. Regarding
 249 Zr, no significant difference between normal conditions and Coastal El Niño was observed in E2 and E5 Callao. However, we
 250 found higher average Zr concentrations for E2 (46 ± 9 ppm) compared with for E5 (34 ± 3 ppm) because the E2 station was

251 closer to the coast and received more sandy inputs. Finally, the Ti/Zr ratio was 1.7 times higher during the Coastal El Niño
252 (April 2017) with to normal conditions at E2.



253
254
255 Figure 5. Al, Ti, and Zr concentration values in ppm and Ti/Zr ratio of surface samples collected at Callao stations. Gray:
256 E2 stations (92m depth), Black: E5 station (178m depth).

257
258 The Ti/Zr record of core 106K1, Callao, used as a proxy for fluvial versus. aeolian inputs, shows millennial variability. During
259 HS1, similar to the increment in fine particle abundance (Fig. 3a), Ti/Zr values were higher during late HS1 than during early
260 HS1 (Fig. 7f). During B-A, a decreasing trend in Ti/Zr ratio was reported (Fig. 7f) by the increase in coarse particle abundance
261 (Fig. 3a).

262 4. Discussion

263 4.1 Assignment of end-members

264 The terrigenous materials deposited on the Peruvian margin are transported by rivers and by wind activity, however, there are
265 also other diffused sources like the material produced by coastal erosion transported offshore by marine currents. The
266 terrigenous sediments in Callao and Pisco are multimodal which suggest that different processes are involved in the transport
267 and deposition of these sediments. In both cores, we observed one end-member corresponding to a fine fraction (EM1) and
268 three EMs corresponding to coarse fractions (EM2, EM3 and EM4). A previous study in Pisco used the variations of fine (10

269 μm) and coarse (50 μm and 100 μm) particles as proxies of river discharge and aeolian inputs respectively for the last few
270 centuries (Briceño-Zuluaga et al., 2016). However, the differences in the aeolian sources, shelf and slope morphology, currents
271 intensity, and hydrodynamics between Callao and Pisco, may modify the interpretation of the proxies described by Briceño-
272 Zuluaga et al. (2016).

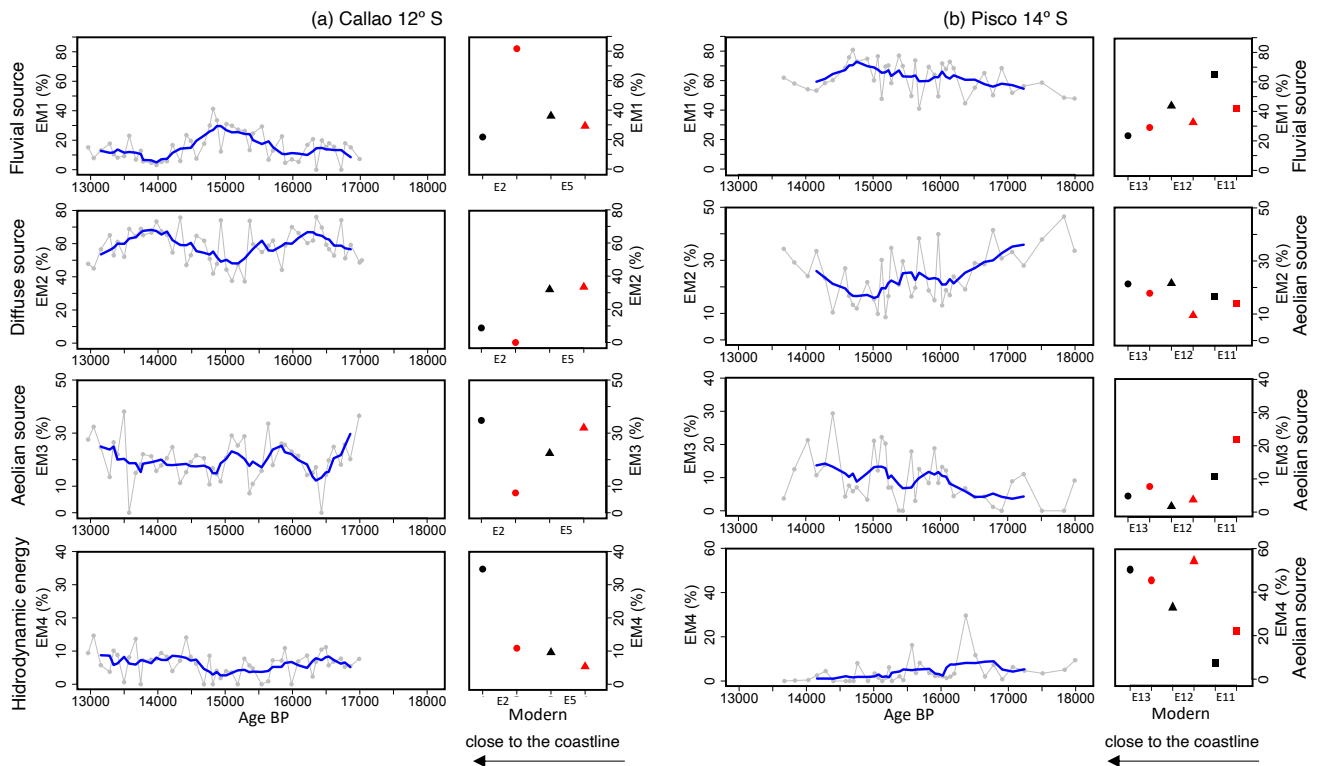
273 EM1 showed a mode at 11 μm and 10 μm in Callao and Pisco, respectively, which is consistent with the grain-size of fine
274 particles (\sim 6-14 μm) in marine sediments associated with river inputs reported in different areas of the world (e.g., Stuut and
275 Lamy, 2004; Stuut et al., 2007; Beuscher et al., 2017) and Pisco (Briceño-Zuluaga et al., 2016). Indeed, the increase of fine
276 particles ($<$ 10 μm) and EM1 contribution in the surface marine sediments from E2 Callao (Fig. 2a and Fig. 6a) associated with
277 local high fluvial discharges in Callao during the 2017 Coastal El Niño (Guzman et al., 2020) corroborates the use of variations
278 in the contribution of EM1 as an indicator of fluvial input changes. The non-increase of fine particles (as well as Al and Ti
279 concentrations) in E5 Callao during Coastal El Niño was probably because of the greater distance between the fluvial source
280 and the sampling site.

281 Previous studies in the South Eastern Pacific used the abundance and fluxes of coarse particles (\sim 36-100 μm) in marine
282 sediments as a proxy for wind intensity linked to the expansion/contraction of the SPSH (e.g., Flores-Aqueveque et al., 2015;
283 Briceño-Zuluaga et al., 2016). Based on HYSPLIT (Hybrid Single-Particle Lagrangian Integrated Trajectory) simulations,
284 Briceño-Zuluaga et al. (2017) have shown that coarse particles (50-90 μm) can directly reach the continental shelf in Pisco
285 during Paracas storms (characterized by wind velocities surpassing 10-15 m/s).

286 The EMs associated with the coarse fraction present similar modes in Callao and Pisco sediments (EM2, \sim 55 μm , EM3, \sim 75
287 μm and EM4, \sim 90-100 μm). Pisco is characterized by a large coastal desert and frequent dust storms. Also, because the shelf
288 at Pisco is narrow, the distance from terrestrial sources that can be transported by winds did not vary significantly during the
289 deglaciation compared with modern conditions. Based on this, particles between 50-90 μm (EM2, EM3 and EM4) can be
290 interpreted as indicators of aeolian input, as proposed by Briceño-Zuluaga et al. (2016). An increase in coarse particle
291 abundance in Pisco surface sediments was recorded at the stations most distant from the coast, E12 and E11, during April 2017
292 (Fig. 2d and 2e), when wind stress along the coast was anomalously enhanced, especially in Central and Southern Peru
293 (Echevin et al., 2018). This observation supports the hypothesis that these particles have an aeolian origin and that the increase
294 of their contribution suggests that, during events with stronger alongshore winds, these particles can be transported to a greater
295 distance than during normal conditions, modifying their proportion in the sediments, but because of the small number of
296 samples, this variation was not statistically significant (Fig. 2d and 2e). Finally, although EM2, EM3 and EM4 reflected an
297 aeolian source, their contributions variations during the last deglaciation were different (Fig. 6b). This can possibly be
298 explained by changes in wind intensity; periods with stronger (weaker) winds result in an increase (decrease) in the amplitude
299 of coarser particles.

300 In Callao, the context is different because there are no large deserts near the coast and dust storms are rare, so is unlikely for
301 \sim 100 μm particles (EM4) to be transported directly to the sampling site. The presence of \sim 100 μm particles could possibly be

302 linked to bottom hydrodynamic processes. Indeed, during events of higher hydrodynamic energy, resuspension of fine particles
 303 and an increase in the relative frequency of coarser particles are expected. EM4 (101 μm) did not show drastic changes during
 304 the last deglaciation, suggesting that it did not influence the relative contribution of the other modes at the millennial-scale
 305 (Fig. 6a). EM2 (58 μm) was found to be the dominant mode in Callao, ranging from 40 to 80% (Fig. 6a). Although these coarse
 306 sediments can be transported by winds (Briceño-Zuluaga et al., 2016, 2017), it is unlikely that this high percentage of coarse
 307 particles could be transported solely by the wind directly to the sampling site off Callao. It is more likely that $\sim 58 \mu\text{m}$ particles
 308 were derived from different sources (winds, coastal erosion) and are distributed on the continental shelf by the Peru-Chile
 309 Undercurrent (Reinhardt et al., 2002). In summary, based on the distance of the sampling site from the aeolian sources, in
 310 addition to the absence of large aeolian sources and dust storms in Callao, we propose that the changes in the contribution of
 311 EM2 and EM4 can be related mainly with other processes associated with diffuse sources and hydrodynamic energy
 312 respectively. Conversely, EM3 can be seen as the best proxy of a wind source.
 313



314
 315 **Figure 6. Variations in the contribution of the grain size end-members from marine cores and surface sediments in Callao (a) and**
 316 **Pisco (b). The modern period is represented by the mean end-member contribution of surface sediments collected during normal**
 317 **conditions (black symbols) and Coastal El Niño April 2017 event (red symbols).**

318

319 4.2. Millennial variability of fluvial and aeolian inputs during the last deglaciation

320 The analysis of EMs allowed for a quantification of the main granulometric modes; however, because the sum of the
321 contribution of the modes corresponds to 100%, it is difficult to consider the modes individually because an increase of one
322 may reduce the others and influence their contribution variability. Thus, for a better visualization, a ratio between EMs
323 indicative of a fluvial (EM1 in Callao and Pisco) and aeolian (EM3 in Callao and the sum of EM2, EM3 and EM4 in Pisco)
324 source will be used as a proxy of the variations in the fluvial and aeolian inputs.

325 An increase in fluvial inputs based on the grain-size and EMA was observed during the Late HS1 (~16-14.7 kyr BP) with
326 maximum values between ~15.5 kyr BP and 14.7 kyr BP in Callao (M77/2-005-3) and Pisco (G14) (Fig. 7g and 7h).

327 Likewise, the Ti /Zr record in Callao (106KL) indicated an increase in fluvial input during HS1, with maximum discharges
328 between ~15.5 kyr BP and 14.9 kyr BP. The increment of Ti in surface sediments during higher fluvial discharges at Callao
329 combined with the good relationship between the Ti/Zr record and the fluvial/aeolian record (EM1/EM3) during the last
330 deglaciation in Callao can support the idea that Ti, which is mostly linked to the fine fraction of marine sediments, is mainly
331 transported by rivers to the Peruvian margin and can be used as a proxy of river discharge and precipitation (e.g., Mollier-
332 Vogel et al., 2013; Salvattecchi et al., 2014; Fleury et al., 2015).

333 The contrasting differences between our record of fluvial input (based on grain size and Ti/Zr) and the record of lithic content
334 based on reflectance (Rein et al., 2005) in Callao can be explained by the difference in the methodology and interpretation of
335 the proxies. Rein et al. (2005) interpret the lithic content as a proxy for river discharges; however, as observed in our data (Fig.
336 6) and the literature (Briceño-Zuluaga et al., 2016), the terrigenous material can be transported to the central-southern Peruvian
337 margin by different sources (e.g., fluvial and aeolian) and the variability of fluvial and aeolian transport follows different
338 patterns, hence responding to different forcing.

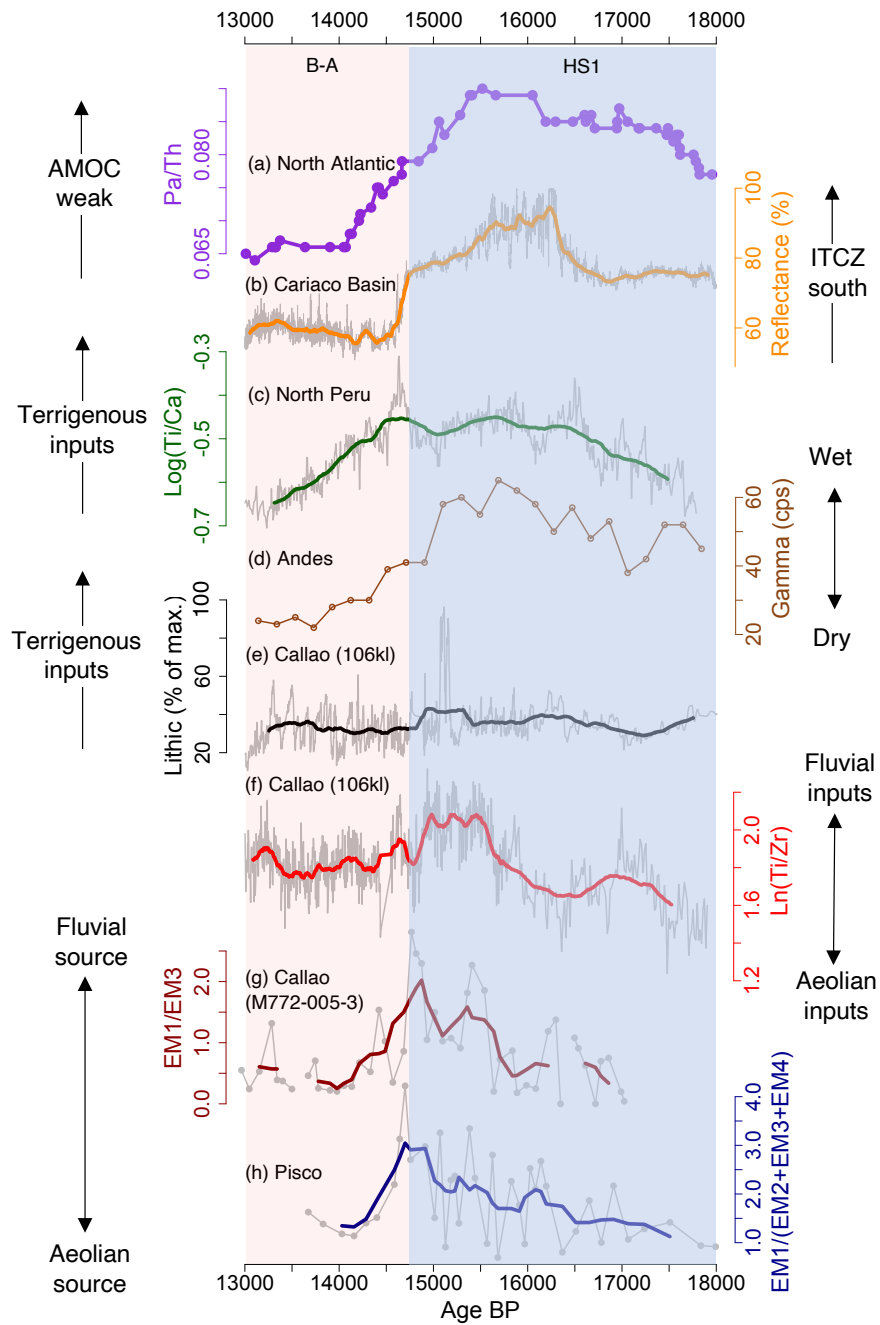
339 Because heavy precipitation associated with the El Niño events in the Callao and Pisco coastal regions are occasional, a larger
340 average fluvial discharge in Callao and Pisco would likely be related to precipitation fluctuations at higher elevations in the
341 watersheds, in the Andes. Previous studies suggest a correlation between North Atlantic cooling and massive meltwater
342 discharges with increased precipitation in the Central Andes (Baker et al., 2001a, 2001b; Blard et al., 2011, Martin et al., 2018;
343 González-Pinilla et al., 2021). During the last deglaciation, cooling in the North Atlantic and higher meltwater discharges
344 generated a weakening of the AMOC (MacManus et al., 2004; Mulitza et al., 2017; Ng et al., 2018). The latter generated an
345 interhemispheric temperature contrast and an impact on precipitation in the Central Andes associated with a southward shift
346 of the ITCZ and an intensification of the South American Monsoon in different regions: Central Andes (Baker et al., 2001a,
347 2001b; Blard et al., 2011; González-Pinilla et al. 2021), Southeast (Cruz et al. 2005; Strikis et al., 2015) and Southwest Brazil
348 (Novello et al., 2017) and in Western Amazonia (Sublette Mosblech et al., 2012; Cheng et al., 2013). Indeed, the higher river
349 discharges we evidenced in Callao and Pisco during Late HS1 (~16-14.7 kyr BP) occurred simultaneously with the well-dated
350 highstand of the giant paleolake Tauca (~16.6-14.5 kyr BP) (Martin et al., 2018). Therefore, the increase and decrease in river

351 discharges in central Peru during HS1 and B-A, respectively, could be explained by changes in precipitation in the Andes in
352 response to changes in the intensity of the AMOC and meltwater pulses in the North Atlantic.
353 During the past few decades, the ITCZ in the East Pacific has shifted southward in and generally narrowed and strengthened
354 (Zhou et al., 2020). A recent study suggests a narrowing and southward shift of the ITCZ in the Eastern Pacific in response to
355 the SSP3-7.0 scenario by 2100 (Mamalakis et al., 2021). Although there are uncertainties about the effects of current global
356 warming on AMOC intensity, there is evidence of the AMOC slowing over the past century (Rahmstorf et al., 2015; Caesar
357 et al., 2018) and in climate model simulations of future climate change, the AMOC is projected to decline generating a
358 southward displacement of the ITCZ (Bellomo et al., 2021). In the context of global warming, a large-scale precipitation and
359 fluvial discharge increases in Peru related to AMOC decline and southward displacement of the ITCZ should be considered.

360

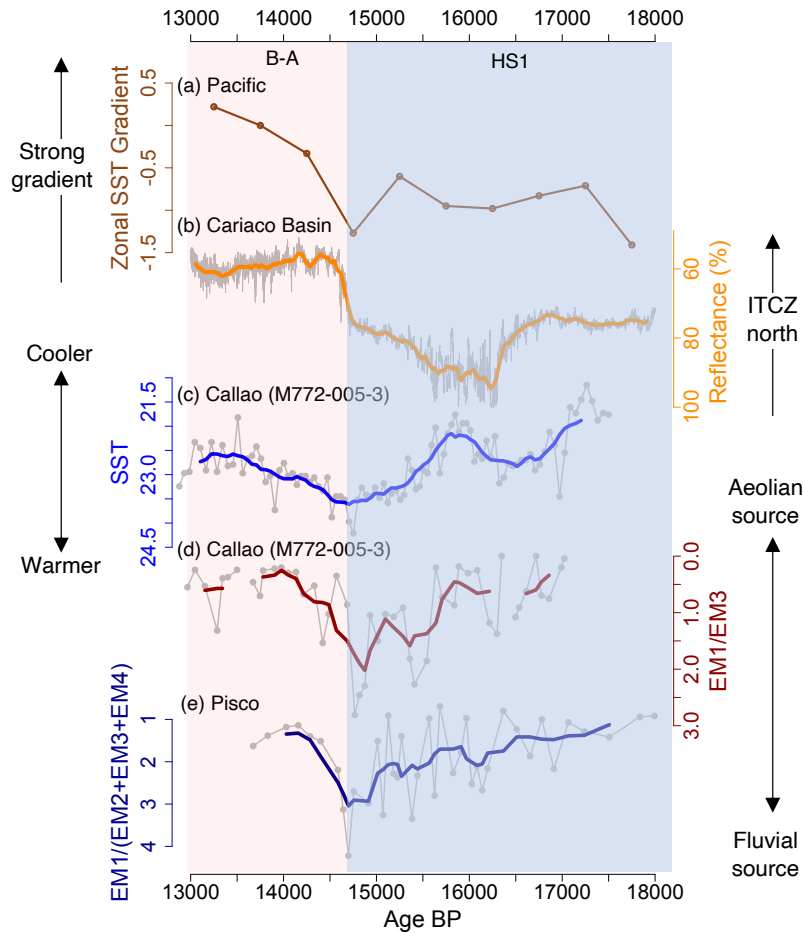
361 Concerning the variations in the aeolian inputs and surface wind intensity in the Peruvian margin, changes in the intensity of
362 Walker circulation and meridional displacements of the ITCZ-SPSH system have been proposed as mechanisms to regulate
363 surface alongshore winds and upwelling dynamics in the Humboldt Current System at multiple timescales (e.g., Gutiérrez et
364 al., 2009; Briceño-Zuluaga et al., 2016; Salvattecí et al., 2014, 2019). On centennial timescales, a northern displacement of the
365 SPSH-ITCZ, here response to stronger Walker circulation, will an increase of alongshore winds and upwelling in Central-
366 South Peruvian margin (Salvattecí et al., 2014; Briceño-Zuluaga et al., 2016). An SST gradient increase in the equatorial
367 Pacific indicates a more intense Walker circulation in B-A than during HS1 (Fig. 8a) (Koutavas and Joanides, 2012). Moreover,
368 a northern displacement of the ITCZ has also been recorded during B-A. (Peterson et al., 2000; Deplazes et al., 2013). These
369 conditions should have provoked an increase of the alongshore winds and aeolian supply in central Peru during B-A. Indeed,
370 in Callao and Pisco, the aeolian inputs were the main transport from 14.7 to 13 kyr BP, suggesting, at least at the regional-
371 scale, an increase of alongshore wind and upwelling in Central-South Peru and an expansion of the SPSH (Fig. 8d and 8e).
372 Our record of surface wind intensity variations and an alkenone-derived SST reconstruction based on alkenones (Salvattecí et
373 al., 2019) in the same core collected from Callao showed similar trends (Fig. 8c). During HS1, a short cooling event between
374 16 and 15.5 kyr BP, coincided with stronger alongshore winds (Fig. 8c and d). And, during the B-A, a cooling at 14.7-13 kyr
375 BP, stronger aeolian transport associated with more intense alongshore winds occurred (Fig. 8c and 8d). These observations
376 suggest that local processes as upwelling variations in response to changes in alongshore wind intensity may control SST
377 variations during the last deglaciation, in addition to other processes such as the advection of the Southern Ocean and Antarctic
378 climate signals by the Humboldt Current.

379



380

381 **Figure 7. (a) Composite $^{231}\text{Pa}/^{230}\text{Th}$ record that reflect past changes in AMOC (Ng et al., 2018). (b) Reflectance (%) from Cariaco**
 382 **Basin as a proxy for the latitudinal displacement of the ITCZ (Deplazes et al., 2013). (c) $\text{Log}(\text{Ti}/\text{Ca})$ for core M77/2-059 from**
 383 **Northern Peru (4°S) (Mollier-Vogel et al., 2003). (d) Natural γ -radiation as a proxy for effective moisture in the Tropical Andes**
 384 **(Baker et al., 2021b). (e) Relative concentration of lithics for core 106Kl from Callao (Rein et al, 2005). (f) $\text{Ln}(\text{Ti}/\text{Zr})$ as a proxy for**
 385 **fluvial vs. aeolian inputs in core 106KL from Callao (this study). (g) $\text{EM1}/\text{EM2}$ ratio as a proxy for fluvial and aeolian source in**
 386 **Callao (this study). (h) $\text{EM1}/(\text{EM2}+\text{EM3}+\text{EM4})$ ratio as a proxy for fluvial and aeolian sources in Pisco (this study).**



388

389 **Figure 8. (a) Zonal SST gradient anomaly during the last deglaciation, here calculated as the difference between Western and**
 390 **Eastern Pacific averages (Koutavas and Joanides, 2012). (b) Reflectance (%) from the Cariaco Basin as a proxy for the latitudinal**
 391 **displacement of the ITCZ (Deplazes et al., 2013). (c) Alkenone-derived near surface temperature from M772-005-3 core, Callao**
 392 **(Salvatteci et al., 2019). (d) EM1/EM2 ratio (Reversal scale) as a proxy for fluvial and aeolian source in Callao (this study). (e)**
 393 **EM1/(EM2+EM3+EM4) ratio (Reversal scale) as a proxy for fluvial and aeolian sources in Pisco (this study).**

394 5. Conclusion

395 The variability of the grain size distribution of marine sediments from the central-southern Peruvian margin (12°S and 14°S)
 396 reveals millennial-scale changes in the transport and sedimentation processes of the terrigenous material during the last
 397 deglaciation (18-13 kyr BP). We identified four granulometric EMs for both Callao and Pisco sediments, each of them
 398 reflecting different processes and sources and whose interpretation must take into consideration regional contexts. In the case
 399 of the Pisco core, located within the range of the aeolian inputs, as it has been shown earlier, the modes (EM2 to EM4)
 400 corresponded to aeolian origin. In the case of the Callao core, which was located further from the coast and where sources of

401 eolian particles are scarce, the EM2 and EM4 modes have been interpreted as reflecting local hydrodynamics, while EM3
402 represented the eolian supply. Our results support a tight relationship between high latitude forcing and precipitation in the
403 western flank of the Andes during the last deglaciation. During late HS1 (16-15 kyr BP), enhanced fluvial inputs in Callao and
404 Pisco occurred and were associated with higher precipitation in the Central Andes in response to the slowdown of AMOC and
405 meltwater discharge in the North Atlantic. Finally, the increase in the aeolian input during the B-A, could be a result of stronger
406 alongshore winds linked to a northern displacement of the ITCZ-SPSH system in response to a strong gradient of the Walker
407 circulation. There is still uncertainty about the effects of current climate change; however, there is evidence of a slowing of
408 the AMOC over the past century and in future climate model simulations. In the latter, the decline in the AMOC is accompanied
409 by a southward shift in the ITCZ. Thus, we can probably expect an increase in precipitation and river flow in Peru in the future.

410 411 Data availability

412 The data associated with this manuscript will be submitted in the PANGAEA database upon publication of this paper.

413

414 Author contributions

415 MY, BT and DG designed the study. MY and SC carried out the grain-size analysis. DG and GS conducted the XRF analysis
416 of core KL 106. FV collected the surficial sample, prepared them and contributed to their interpretation. MY wrote the
417 manuscript with the help of BT and SC. All authors discussed and commented on the paper.

418

419 Competing interests

420 The authors declare that they have no conflict of interests.

421

422 Acknowledgements

423 This publication was made possible through support provided by the IRD-DPF and the MAGNET Program of CONCYTEC
424 N°007-2017. This work was supported by the International Joint Laboratory “PALEOTRACES” (IRD, France; UPMC, France;
425 UFF, Brazil; UA, Chile; UPCH, Peru) and ANR-15-JCLI-0003-03 BELMONT FORUM PACMEDY. Grain-size analyses and
426 ICP-MS analysis were performed on the ALYSES facility (IRD-Sorbonne University, Bondy, France), which is supported by
427 grants from Région Ile-de-France. We thank Irina Djouraev for the sediment preparation and ICP-MS analysis. This work is a
428 contribution of the Collaborative Research Project 754 “Climate-Biogeochemistry interactions in the Tropical Ocean”
429 (www.sfb754.de), which is supported by the Deutsche Forschungsgemeinschaft (DFG). We would like to thank the crew and
430 scientists aboard R/V Meteor cruises M77/2 in 2008. We deeply thank Bo Thamdrup, chief scientist of the Galathea-3
431 expedition (Leg 14), and Bente Lomstein, who conducted the core sampling onboard the RV Vaedderen.

432

433 References

- 434 Bahr, A., Hoffmann, J., Schönfeld, J., Schmidt, M., Nürnberg, D., Batenburg, S. and Voigt, S.: Low-latitude expressions of
435 high-latitude forcing during Heinrich Stadial 1 and the Younger Dryas in northern South America, *Global and Planetary*
436 *Change*, 160, 1-9, doi:10.1016/j.gloplacha.2017.11.008, 2018.
- 437 Baker, P. A., Seltzer, G. O., Fritz, S. C., Dunbar, R. B., Grove, M. J., Tapia, P. M., Cross, S. L., Rowe, H. D. and Broda, J. P.:
438 The History of South American Tropical Precipitation for the Past 25,000 Years. *Science*, 291(5504), 640–643,
439 doi:10.1126/science.291.5504.640, 2001a.
- 440 Baker, P., Rigsby, C., Seltzer, G., Fritz, S., Lowenstein, T., Bacher, N. and Veliz, C.: Tropical climate changes at millennial
441 and orbital timescales on the Bolivian Altiplano, *Nature*, 409(6821), 698-701, doi:10.1038/35055524, 2001b.
- 442 Blard, P., Sylvestre, F., Tripathi, A., Claude, C., Causse, C., Coudrain, A., Condom, T., Seidel, J., Vimeux, F., Moreau, C.,
443 Dumoulin, J. and Lavé, J.: Lake highstands on the Altiplano (Tropical Andes) contemporaneous with Heinrich 1 and the
444 Younger Dryas: new insights from ^{14}C , U–Th dating and $\delta^{18}\text{O}$ of carbonates, *Quaternary Science Reviews*, 30(27-28), 3973-
445 3989, doi:10.1016/j.quascirev.2011.11.001, 2011.
- 446 Beuscher, S., Krüger, S., Ehrmann, W., Schmiedl, G., Milker, Y., Arz, H. and Schulz, H.: End-member modelling as a tool for
447 climate reconstruction—An Eastern Mediterranean case study, *PLoS ONE*, 12(9), e0185136,
448 doi:10.1371/journal.pone.0185136, 2017.
- 449 Bellomo, K., Angeloni, M., Corti, S. and von Hardenberg, J.: Future climate change shaped by inter-model differences in
450 Atlantic meridional overturning circulation response, *Nature Communications*, 12(1), doi:10.1038/s41467-021-24015-w,
451 2021.
- 452 Bourrel, L., Rau, P., Dewitte, B., Labat, D., Lavado, W., Coutaud, A., Vera, A., Alvarado, A. and Ordoñez, J.: Low-frequency
453 modulation and trend of the relationship between ENSO and precipitation along the northern to centre Peruvian Pacific coast,
454 *Hydrological Processes*, 29(6), 1252-1266, doi:10.1002/hyp.10247, 2014.
- 455 Briceño-Zuluaga, F. J., Sifeddine, A., Caquineau, S., Cardich, J., Salvattecchi, R., Gutierrez, D., Ortlieb, L., Velazco, F., Boucher,
456 H. and Machado, C.: Terrigenous material supply to the Peruvian central continental shelf (Pisco, 14° S) during the last 1000
457 years: paleoclimatic implications, *Clim. Past*, 12(3), 787–798, doi:10.5194/cp-12-787-2016, 2016.
- 458 Briceño-Zuluaga, F., Castagna, A., Rutllant, J. A., Flores-Aqueveque, V., Caquineau, S., Sifeddine, A., Velazco, F., Gutierrez,
459 D. and Cardich, J.: Paracas dust storms: Sources, trajectories and associated meteorological conditions, *Atmospheric*
460 *Environment*, 165, 99–110, doi:10.1016/j.atmosenv.2017.06.019, 2017.
- 461 Caesar, L., Rahmstorf, S., Robinson, A., Feulner, G. and Saba, V.: Observed fingerprint of a weakening Atlantic Ocean
462 overturning circulation, *Nature*, 556(7700), 191-196, doi:10.1038/s41586-018-0006-5, 2018.
- 463 Chamorro, A., Echevin, V., Colas, F., Oerder, V., Tam, J. and Quispe-Ccalluari, C.: Mechanisms of the intensification of the
464 upwelling-favorable winds during El Niño 1997–1998 in the Peruvian upwelling system, *Climate Dynamics*, 51(9-10), 3717-
465 3733, doi:10.1007/s00382-018-4106-6, 2018.

466 Cheng, H., Sinha, A., Cruz, F., Wang, X., Edwards, R., d'Horta, F., Ribas, C., Vuille, M., Stott, L. and Auler, A.: Climate
467 change patterns in Amazonia and biodiversity, *Nature Communications*, 4(1), doi:10.1038/ncomms2415, 2013.

468 Cheng, H., Sinha, A., Wang, X., Cruz, F. W. and Edwards, R. L.: The Global Paleomonsoon as seen through speleothem
469 records from Asia and the Americas, *Clim Dyn*, 39(5), 1045–1062, doi:10.1007/s00382-012-1363-7, 2012.

470 Clark, P. U., Shakun, J. D., Baker, P. A., Bartlein, P. J., Brewer, S., Brook, E., Carlson, A. E., Cheng, H., Kaufman, D. S. and
471 Liu, Z.: Global climate evolution during the last deglaciation, *Proceedings of the National Academy of Sciences*, 109(19),
472 E1134–E1142, doi:10.1073/pnas.1116619109, 2012.

473 Cruz, F. W., Burns, S. J., Karmann, I., Sharp, W. D., Vuille, M., Cardoso, A. O., Ferrari, J. A., Silva Dias, P. L. and Viana,
474 O.: Insolation-driven changes in atmospheric circulation over the past 116,000 years in subtropical Brazil, *Nature*, 434(7029),
475 63–66, doi:10.1038/nature03365, 2005.

476 Deplazes, G., Lückge, A., Peterson, L. C., Timmermann, A., Hamann, Y., Hughen, K. A., Röhl, U., Laj, C., Cane, M. A. and
477 Sigman, D. M.: Links between tropical rainfall and North Atlantic climate during the last glacial period, *Nature Geosci*, 6(3),
478 213–217, doi:10.1038/ngeo1712, 2013.

479 Dewitte, B., Illig, S., Renault, L., Goubanova, K., Takahashi, K., Gushchina, D., Mosquera, K. and Purca, S.: Modes of
480 covariability between sea surface temperature and wind stress intraseasonal anomalies along the coast of Peru from satellite
481 observations (2000–2008), *Journal of Geophysical Research*, 116(C4), doi:10.1029/2010jc006495, 2011.

482 Dypvik, H. and Harris, N.: Geochemical facies analysis of fine-grained siliciclastics using Th/U, Zr/Rb and (Zr+Rb)/Sr ratios,
483 *Chemical Geology*, 181(1-4), 131-146, doi:10.1016/s0009-2541(01)00278-9, 2001.

484 Echevin, V., Colas, F., Espinoza-Morriberon, D., Vasquez, L., Anculle, T. and Gutierrez, D.: Forcings and Evolution of the
485 2017 Coastal El Niño Off Northern Peru and Ecuador, *Frontiers in Marine Science*, 5, doi:10.3389/fmars.2018.00367, 2018.

486 Fleury, S., Martinez, P., Crosta, X., Charlier, K., Billy, I., Hanquiez, V., Blanz, T. and Schneider, R. R.: Pervasive multidecadal
487 variations in productivity within the Peruvian Upwelling System over the last millennium, *Quat. Sci. Rev.*, 125, 78–90,
488 doi:10.1016/j.quascirev.2015.08.006, 2015.

489 Flores-Aqueveque, V., Alfaro, S., Vargas, G., Rutllant, J. A. and Caquineau, S.: Aeolian particles in marine cores as a tool for
490 quantitative high-resolution reconstruction of upwelling favorable winds along coastal Atacama Desert, Northern Chile, *Prog.*
491 *Oceanogr.*, 134, 244–255, doi:10.1016/j.pocean.2015.02.003, 2015.

492 Flores-Aqueveque, V., Caquineau, S., Alfaro, S., Valdes, J. and Vargas, G.: Using Image-Based Size Analysis For Determining
493 the Size Distribution and Flux of Eolian Particles Sampled In Coastal Northern Chile (23 S), *Journal of Sedimentary Research*,
494 84(4), 238-244, doi:10.2110/jsr.2014.23, 2014.

495 Garreaud, R., Vuille, M., Compagnucci, R. and Marengo, J.: Present-day South American climate, *Palaeogeography*,
496 *Palaeoclimatology, Palaeoecology*, 281(3-4), 180-195, doi:10.1016/j.palaeo.2007.10.032, 2009.

497 González-Pinilla, F., Latorre, C., Rojas, M., Houston, J., Rocuant, M., Maldonado, A., Santoro, C., Quade, J. and Betancourt,
498 J.: High- and low-latitude forcings drive Atacama Desert rainfall variations over the past 16,000 years, *Science Advances*,
499 7(38), doi:10.1126/sciadv.abg1333, 2021.

500 Gutiérrez, D., Bouloubassi, I., Sifeddine, A., Purca, S., Goubanova, K., Graco, M., Field, D., Méjanelle, L., Velazco, F., Lorre,
501 A., Salvattecchi, R., Quispe, D., Vargas, G., Dewitte, B. and Ortlieb, L.: Coastal cooling and increased productivity in the main
502 upwelling zone off Peru since the mid-twentieth century, *Geophys. Res. Lett.*, 38(7), doi:10.1029/2010GL046324, 2011.

503 Gutiérrez, D., Sifeddine, A., Field, D., Ortlieb, L., Vargas, G., Chávez, F., Velazco, F., Ferreira, V., Tapia, P., Salvattecchi, R.,
504 Boucher, H., Morales, M., Valdés, J., Reyss, J., Campusano, A., Boussafir, M., Mandeng-Yogo, M., García, M. and
505 Baumgartner, T.: Rapid reorganization in ocean biogeochemistry off Peru towards the end of the Little Ice Age,
506 *Biogeosciences*, 6(5), 835-848, doi:10.5194/bg-6-835-2009, 2009.

507 Gutiérrez, D., Sifeddine, A., Reyss, J. L., Vargas, G., Velazco, F., Salvattecchi, R., Ferreira, V., Ortlieb, L., Field, D.,
508 Baumgartner, T., Boussafir, M., Boucher, H., Valdés, J., Marinovic, L., Soler, P. and Tapia, P.: Anoxic sediments off Central
509 Peru record interannual to multidecadal changes of climate and upwelling ecosystem during the last two centuries, *Adv.*
510 *Geosci.*, 6, 119–125, doi:10.5194/adgeo-6-119-2006, 2006.

511 Guzman, E., Ramos, C. and Dastgheib, A.: Influence of the El Niño Phenomenon on Shoreline Evolution. Case Study: Callao
512 Bay, Perú, *Journal of Marine Science and Engineering*, 8(2), 90, doi:10.3390/jmse8020090, 2020.

513 Haug, G., Hughen, K., Sigman, D., Peterson, L. and Röhl, U.: Southward Migration of the Intertropical Convergence Zone
514 Through the Holocene, *Science*, 293(5533), 1304-1308, doi:10.1126/science.1059725, 2001.

515 Holz, C., Stuut, J. B. W., Henrich, R. and Meggers, H.: Variability in terrigenous sedimentation processes off northwest Africa
516 and its relation to climate changes: Inferences from grain-size distributions of a Holocene marine sediment record, *Sediment.*
517 *Geol.*, 202(3), 499–508, doi:10.1016/j.sedgeo.2007.03.015, 2007.

518 Humphries, M. S., Benitez-Nelson, C. R., Bizimis, M. and Finch, J. M.: An aeolian sediment reconstruction of regional wind
519 intensity and links to larger scale climate variability since the last deglaciation from the east coast of southern Africa, *Global*
520 *and Planetary Change*, 156, 59–67, doi:10.1016/j.gloplacha.2017.08.002, 2017.

521 Jansen, J., Van der Gaast, S., Koster, B. and Vaars, A.: CORTEX, a shipboard XRF-scanner for element analyses in split
522 sediment cores, *Marine Geology*, 151(1-4), 143-153, doi:10.1016/s0025-3227(98)00074-7, 1998.

523 Jarvis, K. E., A. L. Gray, and R. S. Houk. *Handbook of Inductively Coupled Plasma Mass Spectrometry*. Blackie Academic
524 & Professional, an imprint of Chapman & Hall, Wester Cleddens Road, Bishopgriggs, Glasgow, London Glasgow New York
525 Tokyo Merlbourne Madras, 1992.

526 Jiang, H., Zhong, N., Li, Y., Ma, X., Xu, H., Shi, W., Zhang, S. and Nie, G.: A continuous 13.3-ka record of seismogenic dust
527 events in lacustrine sediments in the eastern Tibetan Plateau, *Sci Rep*, 7(1), doi:10.1038/s41598-017-16027-8, 2017.

528 Just, J., Heslop, D., von Dobeneck, T., Bickert, T., Dekkers, M. J., Frederichs, T., Meyer, I. and Zabel, M.: Multiproxy
529 characterization and budgeting of terrigenous end-members at the NW African continental margin, *Geochem. Geophys.*
530 *Geosyst.*, 13(9), doi:10.1029/2012GC004148, 2012.

531 Koutavas, A. and Joanides, S.: El Niño-Southern Oscillation extrema in the Holocene and Last Glacial Maximum,
532 *Paleoceanography*, 27(4), doi:10.1029/2012pa002378, 2012.

533 Lagos, P., Silva, Y., Nickl, E. and Mosquera, K.: El Niño – related precipitation variability in Perú, *Advances in Geosciences*,
534 14, 231-237, doi:10.5194/adgeo-14-231-2008, 2008.

535 Mamalakis, A., Randerson, J., Yu, J., Pritchard, M., Magnusdottir, G., Smyth, P., Levine, P., Yu, S. and Foufoula-Georgiou,
536 E.: Zonally contrasting shifts of the tropical rain belt in response to climate change, *Nature Climate Change*, 11(2), 143-151,
537 doi:10.1038/s41558-020-00963-x, 2021.

538 Martin, L. C. P., Blard, P. H., Lavé, J., Condom, T., Prémaillon, M., Jomelli, V., Brunstein, D., Lupker, M., Charreau, J.,
539 Mariotti, V., Tibari, B., Team, A. and Davy, E.: Lake Tauca highstand (Heinrich Stadial 1a) driven by a southward shift of the
540 Bolivian High, *Sci. Adv.*, 4(8), doi:10.1126/sciadv.aar2514, 2018.

541 McGee, D., Donohoe, A., Marshall, J. and Ferreira, D.: Changes in ITCZ location and cross-equatorial heat transport at the
542 Last Glacial Maximum, Heinrich Stadial 1, and the mid-Holocene, *Earth Planet. Sci. Lett.*, 390, 69–79,
543 doi:10.1016/j.epsl.2013.12.043, 2014.

544 McManus, J. F., Francois, R., Gherardl, J. M., Kelgwin, L. and Drown-Leger, S.: Collapse and rapid resumption of Atlantic
545 meridional circulation linked to deglacial climate changes, *Nature*, 428(6985), 834–837, doi:10.1038/nature02494, 2004.

546 Mollier-Vogel, E., Leduc, G., Bösch, T., Martinez, P. and Schneider, R. R.: Rainfall response to orbital and millennial
547 forcing in northern Peru over the last 18ka, *Quat. Sci. Rev.*, 76, 29–38, doi:10.1016/j.quascirev.2013.06.021, 2013.

548 Montade, V., Kageyama, M., Combourieu-Nebout, N., Ledru, M. P., Michel, E., Siani, G. and Kissel, C.: Teleconnection
549 between the intertropical convergence zone and southern westerly winds throughout the last deglaciation, *Geology*, 43(8),
550 735–738, doi:10.1130/G36745.1, 2015.

551 Morera, S., Condom, T., Crave, A., Steer, P. and Guyot, J.: The impact of extreme El Niño events on modern sediment transport
552 along the western Peruvian Andes (1968–2012), *Scientific Reports*, 7(1), doi:10.1038/s41598-017-12220-x, 2017.

553 Mulitza, S., Chiessi, C. M., Schefuß, E., Lippold, J., Wichmann, D., Antz, B., Mackensen, A., Paul, A., Prange, M., Rehfeld,
554 K., Werner, M., Bickert, T., Frank, N., Kuhnert, H., Lynch-Stieglitz, J., Portilho-Ramos, R. C., Sawakuchi, A. O., Schulz, M.,
555 Schwenk, T., Tiedemann, R., Vahlenkamp, M. and Zhang, Y.: Synchronous and proportional deglacial changes in Atlantic
556 meridional overturning and northeast Brazilian precipitation, *Paleoceanography*, 32(6), 622–633, doi:10.1002/2017PA003084,
557 2017.

558 Ng, H. C., Robinson, L. F., McManus, J. F., Mohamed, K. J., Jacobel, A. W., Ivanovic, R. F., Gregoire, L. J. and Chen, T.:
559 Coherent deglacial changes in western Atlantic Ocean circulation, *Nat Commun*, 9(1), doi:10.1038/s41467-018-05312-3,
560 2018.

561 Novello, V. F., Cruz, F. W., Vuille, M., Strikis, N. M., Edwards, R. L., Cheng, H., Emerick, S., de Paula, M. S., Li, X., Barreto,
562 E. de S., Karmann, I. and Santos, R. V.: A high-resolution history of the South American Monsoon from Last Glacial Maximum
563 to the Holocene, *Sci. Rep.*, 7(March), 44267, doi:10.1038/srep44267, 2017.

564 Ortlieb, L., Vargas, G. and Sali??ge, J. F.: Marine radiocarbon reservoir effect along the northern Chile-southern Peru coast
565 (14-24??S) throughout the Holocene, *Quat. Res.*, 75(1), 91–103, doi:10.1016/j.yqres.2010.07.018, 2011.

566 Paterson, G. A. and Heslop, D.: New methods for unmixing sediment grain size data, *Geochem. Geophys. Geosyst.*, 16(12),
567 4494–4506, doi:10.1002/2015GC006070, 2015.

568 Peterson, L., Haug, G., Hughen, K. and Röhl, U.: Rapid Changes in the Hydrologic Cycle of the Tropical Atlantic During the
569 Last Glacial, *Science*, 290(5498), 1947-1951, doi:10.1126/science.290.5498.1947, 2000.

570 Pettijohn, F.: Persistence of Heavy Minerals and Geologic Age, *The Journal of Geology*, 49(6), 610-625, doi:10.1086/624992,
571 1941.

572 Pichevin, L., Cremer, M., Giraudeau, J. and Bertrand, P.: A 190 ky record of lithogenic grain-size on the Namibian slope:
573 Forging a tight link between past wind-strength and coastal upwelling dynamics, *Mar. Geol.*, 218(1–4), 81–96,
574 doi:10.1016/j.margeo.2005.04.003, 2005.

575 Rahmstorf, S., Box, J., Feulner, G., Mann, M., Robinson, A., Rutherford, S. and Schaffernicht, E.: Exceptional twentieth-
576 century slowdown in Atlantic Ocean overturning circulation, *Nature Climate Change*, 5(5), 475-480,
577 doi:10.1038/nclimate2554, 2015.

578 Rahn, D. and Garreaud, R.: A synoptic climatology of the near-surface wind along the west coast of South America,
579 *International Journal of Climatology*, 34(3), 780-792, doi:10.1002/joc.3724, 2013.

580 Rau, P., Bourrel, L., Labat, D., Melo, P., Dewitte, B., Frappart, F., Lavado, W. and Felipe, O.: Regionalization of rainfall over
581 the Peruvian Pacific slope and coast, *International Journal of Climatology*, 37(1), 143-158, doi:10.1002/joc.4693, 2016.

582 Rein, B., Lückge, A. and Sirocko, F.: A major Holocene ENSO anomaly during the Medieval period, *Geophysical Research*
583 *Letters*, 31(17), doi:10.1029/2004gl020161, 2004.

584 Rein, B., Lückge, A., Reinhardt, L., Sirocko, F., Wolf, A. and Dullo, W. C.: El Niño variability off Peru during the last 20,000
585 years, *Paleoceanography*, 20(4), 1–18, doi:10.1029/2004PA001099, 2005.

586 Reinhardt, L., Kudrass, H. R., Lückge, A., Wiedicke, M., Wunderlich, J., & Wendt, G.: High-resolution sediment
587 echosounding off Peru: Late Quaternary depositional sequences and sedimentary structures of a current-dominated
588 shelf, *Marine Geophysical Researches*, 23(4), 335-35, 2002

589 Salvatelli, R., Gutiérrez, D., Field, D., Sifeddine, A., Ortlieb, L., Bouloubassi, I., Boussafir, M., Boucher, H. and Cetin, F.:
590 The response of the Peruvian Upwelling Ecosystem to centennial-scale global change during the last two millennia, *Clim.*
591 *Past*, 10(2), 715–731, doi:10.5194/cp-10-715-2014, 2014a.

592 Salvatelli, R., Field, D., Sifeddine, A., Ortlieb, L., Ferreira, V., Baumgartner, T., Caquineau, S., Velazco, F., Reyss, J.,
593 Sanchez-Cabeza, J. and Gutierrez, D.: Cross-stratigraphies from a seismically active mud lens off Peru indicate horizontal
594 extensions of laminae, missing sequences, and a need for multiple cores for high resolution records, *Marine Geology*, 357, 72-
595 89, doi:10.1016/j.margeo.2014.07.008, 2014b.

596 Salvatelli, R., Gutierrez, D., Sifeddine, A., Ortlieb, L., Druffel, E., Boussafir, M. and Schneider, R.: Centennial to millennial-
597 scale changes in oxygenation and productivity in the Eastern Tropical South Pacific during the last 25,000 years, *Quat. Sci.*
598 *Rev.*, 131, 102–117, doi:10.1016/j.quascirev.2015.10.044, 2016.

599 Salvattecchi, R., Schneider, R. R., Blanz, T. and Mollier-Vogel, E.: Deglacial to Holocene Ocean Temperatures in the Humboldt
600 Current System as Indicated by Alkenone Paleothermometry, *Geophys. Res. Lett.*, 46(1), 281–292,
601 doi:10.1029/2018GL080634, 2019.

602 Saukel, C., Lamy, F., Stuut, J. B. W., Tiedemann, R. and Vogt, C.: Distribution and provenance of wind-blown SE Pacific
603 surface sediments, *Mar. Geol.*, 280(1–4), 130–142, doi:10.1016/j.margeo.2010.12.006, 2011.

604 Scheidegger, K. F. and Krissek, L. A.: Dispersal and deposition of eolian and fluvial sediments off Peru and northern Chile.,
605 *Geol. Soc. Am. Bull.*, 93(2), 150–162, doi:10.1130/0016-7606(1982)93<150:DADDOEA>2.0.CO;2, 1982.

606 Shakun, J. D., Clark, P. U., He, F., Marcott, S. A., Mix, A. C., Liu, Z., Otto-Bliesner, B., Schmittner, A. and Bard, E.: Global
607 warming preceded by increasing carbon dioxide concentrations during the last deglaciation, *Nature*, 484(7392), 49–54,
608 doi:10.1038/nature10915, 2012.

609 Sifeddine, A., Gutierrez, D., Ortlieb, L., Boucher, H., Velazco, F., Field, D., Vargas, G., Boussafir, M., Salvattecchi, R., Ferreira,
610 V., García, M., Valdés, J., Caquineau, S., Mandeng Yogo, M., Cetin, F., Solis, J., Soler, P. and Baumgartner, T.: Laminated
611 sediments from the central Peruvian continental slope: A 500 year record of upwelling system productivity, terrestrial runoff
612 and redox conditions, *Prog. Oceanogr.*, 79(2–4), 190–197, doi:10.1016/j.pocean.2008.10.024, 2008.

613 Strikis, N. M., Chiessi, C. M., Cruz, F. W., Vuille, M., Cheng, H., De Souza Barreto, E. A., Mollenhauer, G., Kasten, S.,
614 Karmann, I., Edwards, R. L., Bernal, J. P. and Sales, H. D. R.: Timing and structure of Mega-SACZ events during Heinrich
615 Stadial 1, *Geophys. Res. Lett.*, 42(13), 5477–5484, doi:10.1002/2015GL064048, 2015.

616 Strikis, N., Cruz, F., Barreto, E., Naughton, F., Vuille, M., Cheng, H., Voelker, A., Zhang, H., Karmann, I., Edwards, R., Auler,
617 A., Santos, R. and Sales, H.: South American monsoon response to iceberg discharge in the North Atlantic, *Proceedings of the*
618 *National Academy of Sciences*, 115(15), 3788–3793, doi:10.1073/pnas.1717784115, 2018.

619 Strub, P. T., Mesias, J. M., Montecino, V., Rutllant, J., and Salinas, S.: Coastal ocean circulation off western South America,
620 in: *The Sea*, Vol. 11, edited by: Robinson, A. and Brink, K., John Wiley & Sons, New York, USA, 273–313, 1998.

621 Stuut, J. B. W., Kasten, S., Lamy, F. and Hebbeln, D.: Sources and modes of terrigenous sediment input to the Chilean
622 continental slope, *Quat. Int.*, 161(1), 67–76, doi:10.1016/j.quaint.2006.10.041, 2007.

623 Stuut, J. B. W., Prins, M. A., Schneider, R. R., Weltje, G. J., Fred Jansen, J. H. and Postma, G.: A 300-kyr record of aridity
624 and wind strength in southwestern Africa: Inferences from grain-size distributions of sediments on Walvis Ridge, SE Atlantic,
625 *Mar. Geol.*, 180(1–4), 221–233, doi:10.1016/S0025-3227(01)00215-8, 2002.

626 Stuut, J. B. W., Temmesfeld, F. and De Deckker, P.: A 550ka record of aeolian activity near north west cape, australia:
627 Inferences from grain-size distributions and bulk chemistry of SE indian ocean deep-sea sediments, *Quat. Sci. Rev.*, 83, 83–
628 94, doi:10.1016/j.quascirev.2013.11.003, 2014.

629 Stuut, J.-B. W. and Lamy, F.: Climate variability at the southern boundaries of the Namib (southwestern Africa) and Atacama
630 (northern Chile) coastal deserts during the last 120,000 yr, *Quat. res.*, 62(3), 301–309, doi:10.1016/j.yqres.2004.08.001, 2004.

631 Suess, E., Kulm, L. D. and Killingley, J. S.: Coastal upwelling and a history of organic-rich mudstone deposition off Peru,
632 Geological Society, London, Special Publications, 26(1), 181–197, doi:10.1144/GSL.SP.1987.026.01.11, 1987.

633 Sublette Mosblech, N., Chepstow-Lusty, A., Valencia, B. and Bush, M.: Anthropogenic control of late-Holocene landscapes
634 in the Cuzco region, Peru, *The Holocene*, 22(12), 1361-1372, doi:10.1177/0959683612449760, 2012.

635 Vuille, M., Burns, S., Taylor, B., Cruz, F., Bird, B., Abbott, M., Kanner, L., Cheng, H. and Novello, V.: A review of the South
636 American monsoon history as recorded in stable isotopic proxies over the past two millennia, *Climate of the Past*, 8(4), 1309-
637 1321, doi:10.5194/cp-8-1309-2012, 2012.

638 Weltje, G. J. and Prins, M. A.: Genetically meaningful decomposition of grain-size distributions, *Sedimentary Geology*,
639 202(3), 409–424, doi:10.1016/j.sedgeo.2007.03.007, 2007.

640 Weltje, G. J. and Prins, M. A.: Muddled or mixed? Inferring palaeoclimate from size distributions of deep-sea clastics,
641 *Sedimentary Geology*, 162(1–2), 39–62, doi:10.1016/s0037-0738(03)00235-5, 2003.

642 Wu, L., Wilson, D., Wang, R., Yin, X., Chen, Z., Xiao, W. and Huang, M.: Evaluating Zr/Rb Ratio From XRF Scanning as an
643 Indicator of Grain-Size Variations of Glaciomarine Sediments in the Southern Ocean, *Geochemistry, Geophysics, Geosystems*,
644 21(11), doi:10.1029/2020gc009350, 2020.

645 Yarincik, K., Murray, R. and Peterson, L.: Climatically sensitive eolian and hemipelagic deposition in the Cariaco Basin,
646 Venezuela, over the past 578,000 years: Results from Al/Ti and K/Al, *Paleoceanography*, 15(2), 210-228,
647 doi:10.1029/1999pa900048, 2000.

648 Zhang, Y., Chiessi, C. M., Mulitza, S., Zabel, M., Trindade, R. I. F., Helena, M., Hollanda, B. M., Dantas, E. L., Govin, A.,
649 Tiedemann, R. and Wefer, G.: Origin of increased terrigenous supply to the NE South American continental margin during
650 Heinrich Stadial 1 and the Younger Dryas, *Earth Planet. Sci. Lett.*, 432, 493–500, doi:10.1016/j.epsl.2015.09.054, 2015.

651 Zhou, W., Leung, L., Lu, J., Yang, D. and Song, F.: Contrasting Recent and Future ITCZ Changes From Distinct Tropical
652 Warming Patterns, *Geophysical Research Letters*, 47(22), doi:10.1029/2020gl089846, 2020.

653